Available online at www.sciencedirect.com

ScienceDirect

Energy Procedia 142 (2017) 3667–3674

Energy Procedia

www.elsevier.com/locate/procedia

9th International Conference on Applied Energy, ICAE2017, 21-24 August 2017, Cardiff, UK

Numerical and experimental study of the flow-by cell for Vanadium Redox Batteries

M. Pugach[a,c*], M. Kondratenko[b], S. Briola[a], A. Bischi[a]

[a]*Skolkovo Institute of Science and Technology, Skolkovo Innovation Center, Building 3, Moscow 143026, Russia*
[b]*Lomonosov Moscow State University,GSP-1, Leninskie Gory, Moscow, 119991, Russia*
[c]*Moscow Institute of Physics and Technology, 9 Institutskiy per., Dolgoprudny, Moscow Region, 141701, Russia*

Abstract

A mathematical model for vanadium redox batteries (VRBs) is considered. The model has been tuned using experimental data obtained for a single cell with flow-by design. Mass transfer limitations have been determined from experimental data, and a new correlation for mass transfer constant is proposed. Self-discharge of the battery resulting from crossover of vanadium ions through membrane is taken into account by the model as well. It is shown that Fick's law for diffusion describes crossover rather well. The crossover has a large impact on the battery voltage during discharge, but can be neglected during charge due to mutual compensation of diffusion and migration fluxes. Good agreement (with average error less than 7 %) between the experimental and modelled polarization and charge-discharge curves is observed in the whole current density region.

Peer-review under responsibility of the scientific committee of the 9th International Conference on Applied Energy.

Keywords: numerical simulation; mathematical model; Vanadium redox flow batteries; flow-by design; ion crossover; migration; diffusion; polarization curve; concentration overvoltages

Nomenclature

A_{ch}	electrode channels cross-section area [m^2]	*Greek symbols*	
A_e	electrode surface area [m^2]	ε	membrane porosity [-]
A_m	electrode-membrane interface area [m^2]	η_{act}	activation overvoltage [V]

* Corresponding author. Tel.: +7-967-040-64-01
E-mail address: mikhail.pugach@skolkovotech.ru

1876-6102
Peer-review under responsibility of the scientific committee of the 9th International Conference on Applied Energy .
10.1016/j.egypro.2017.12.260

c	molar concentration [mol L^{-1}]	η_{con}	concentration overvoltage [V]
CE	Coulombic efficiency [-]	η_{ohm}	ohmic overvoltage [V]
D	diffusion coefficient [m^2 s^{-1}]	τ	process duration [s]
d_m	membrane thickness [m]	*Acronyms, subscripts, superscripts*	
EE	energy efficiency [-]	c	charge
F	Faraday constant [C mol^{-1}]	ce	*cell*
G	gas constant [J $K^{-1}mol^{-1}$]	d	discharge
I	current [A]	*eff*	effective
k_m	mass transfer coefficient electrode-electrolyte interface [m s^{-1}]	*ex*	experimental value
		hc	half-cell
Q	electrolyte flow rate [L s^{-1}]	i	i-th vanadium ion
R_{ce}	cell equivalent electric resistance [Ω]	*init*	initial value
t	time [s]	n	simulation time step number
Δt	calculation time step [s]	*ne*	negative electrode
T	ambient temperature [K]	*pe*	positive electrode
u	electrolyte velocity in electrode channel [m/s]	*react*	reactant
U_{ce}	cell voltage [V]	*tk*	tank
$\langle U_{ce} \rangle$	time average cell voltage [V]	*th*	theoretical value
U_{eq}	cell equilibrium potential [V]	*van*	vanadium
U_0	redox couples standard reduction potential [V]	2	V^{2+} ion
V	volume [m^3]	3	V^{3+} ion
VE	voltage efficiency [-]	4	VO^{2+} ion
		5	VO_2^+ ion

1. Introduction

The share of renewable energy sources (e.g. solar and wind) in the world energy consumption is continuously increasing [1]. However, their intermittent nature makes them rather difficult to implement for stable power supply. Electrical Energy Storage (EES) systems are considered to be one of the key technologies that can tackle this problem [2,3]. Among various EES systems, Redox Flow Batteries (RFB) are considered as a promising solution for stationary energy storage due to their strong features [4–6]: long life time (thousands of cycles), deep discharge without risk of damage, modularity and independence of energy and power ratings. Several types of RFB that use different redox couples have been proposed [7,8]. Most of them are under development, while Vanadium Redox Batteries (VRB) demonstrated rather good performance and have already found certain commercial applications [9–11]. Moreover, VRB might be especially interesting for application in Russian energy market, as Russia is one of the top vanadium producers worldwide [12].

The purpose of this study was to develop a semi empirical model of VRB that could reflect the main mechanisms of energy losses and allow to estimate the technical performance of the battery.

2. Operation of VRB

VRB consists of two half-cells that are separated by a polymeric membrane. The half-cells are connected with external tanks, which provide required volume of electrolyte circulated by pumps.

The electrolytes in both tanks are constituted by the vanadium salts dissolved in aqueous solution of sulphuric acid. In charge mode, the electrochemical reaction (1) takes place in the positive electrode, where the transformation of VO^{2+} ion (within the salt $VOSO_4$) into VO_2^+ ion (within the salt $(VO_2)_2SO_4$) occurs with releasing of one electron:

$$VO^{2+} + H_2O \leftrightarrow VO_2^+ + 2H^+ + e^- \quad (1)$$

In the negative electrode in charge mode, the transferred electron transforms the V^{3+} ion (within the salt

$V_2(SO_4)_3$) into the V^{2+} ion (within the salt VSO_4):

$$V^{3+} + e^- \leftrightarrow V^{2+} \tag{2}$$

The two half-cells are separated by the membrane to prevent mixing of positive and negative electrolytes (some vanadium ions can also transfer across the membrane (crossover) leading to side reactions, which result in self-discharge of the battery). The membrane is permeable for protons, as protons exchange between two half-cells completes the electrochemical circuit and provides continuous occurrence of electrochemical reactions (1) and (2). Thus, in charge mode one of two protons generated in reaction (1) transfers to the opposite half-cell. In discharge mode, the overall processes, including the reactions (1) and (2), take place in the opposite direction.

3. Model

The proposed mathematical model allows to determine the voltage ($U_{ce}(t)$) and the state of charge ($SOC(t)$) of a single VRB flow-by cell [13] during charge and discharge processes, depending on the operating conditions: current ($I(t)$), electrolyte flow rate ($Q(t)$) and ambient temperature (T).

In order to derive the mathematical model for a single cell, the following assumptions were made:

1) Physical properties of electrodes, electrolyte and membrane are isotropic and homogeneous [14];
2) All domains work under isothermal conditions [14];
3) The cells and tanks behave as continuous stirred tank reactors [15];
4) Concentrations change linearly across the membrane and there are no reactions taking place in the membrane [14];
5) The value of concentration on the surface of the membrane is equal to its value in the half-cell from the same side, while on the other side the value of this concentration is equal to zero due to rapid oxidation/reduction of corresponding vanadium species diffused through the membrane [16];
6) Cell electric resistance remains constant over the operating SOC range of the VRB [15].

The $U_{ce}(t)$ is calculated as algebraic sum (positive and negative sign are related to the charge and discharge processes, respectively) of the equilibrium potential and internal losses, which are presented by activation, ohmic and concentration overvoltages [17]:

$$U_{ce}(t) = U_{eq}(t) \pm \left(\eta_{act}(t) + \eta_{ohm}(t) + \eta_{con}(t)\right) \tag{3}$$

The equilibrium conditions take place when there is no current flow in the cell. The $U_{eq}(t)$ can be described by Nernst equation [17]:

$$U_{eq}(t) = U_0 + \frac{GT}{F} ln\left\{\left(\frac{c_2^{hc}(t)}{c_3^{hc}(t)}\right)\left(\frac{c_5^{hc}(t)\cdot\left(c_{H^+}^{hc}(t)\right)^2}{c_4^{hc}(t)}\right)\right\} \tag{4}$$

Concentrations of vanadium species in the cell can be calculated according to Eq. (5) [15,18,19]:

$$\begin{pmatrix} c_2^{hc}(t) \\ c_3^{hc}(t) \\ c_4^{hc}(t) \\ c_5^{hc}(t) \end{pmatrix}^{n+1} = \begin{pmatrix} c_2^{hc}(t) \\ c_3^{hc}(t) \\ c_4^{hc}(t) \\ c_5^{hc}(t) \end{pmatrix}^{n} \pm \frac{I(t)\Delta t}{V_{tk}F}\begin{pmatrix} 1 \\ -1 \\ -1 \\ 1 \end{pmatrix} + \frac{A_e \Delta t}{d_m V_{hc}}\begin{pmatrix} -D_2^{eff} & 0 & -D_4^{eff} & -2D_5^{eff} \\ 0 & -D_3^{eff} & +2D_4^{eff} & +3D_5^{eff} \\ +3D_2^{eff} & +2D_3^{eff} & -D_4^{eff} & 0 \\ -2D_2^{eff} & -D_3^{eff} & 0 & -D_5^{eff} \end{pmatrix}\begin{pmatrix} c_2^{hc}(t) \\ c_3^{hc}(t) \\ c_4^{hc}(t) \\ c_5^{hc}(t) \end{pmatrix}^{n} \tag{5}$$

where D_i^{eff} is effective coefficient of diffusion, which is different from intrinsic value D_i due to the influence of porosity of the membrane and was calculated with application of Bruggeman correlation [20]:

$$D_i^{eff} = \varepsilon^{3/2} D_i \tag{6}$$

In the Eq. (5) the first summand presents the concentration on the current time step, the second term reflects the Faraday's law [18], the last term allows for crossover [19]. The crossover occurs due to diffusion of vanadium ions

though the membrane from one half-cell to the opposite one. Diffusion of V^{2+} and V^{3+} ions from negative side lead to their reactions with VO_2^+ and VO^{2+} in the positive half-cell [15]:

$$V^{2+} + 2VO_2^+ + 2H^+ \rightarrow 3VO^{2+} + H_2O \quad (7) \qquad V^{3+} + VO_2^+ \rightarrow 2VO^{2+} \quad (8)$$

At the same time, diffusion of VO_2^+ and VO^{2+} ions from the positive side lead to their reactions with V^{2+} and V^{3+} in the negative half-cell [15]:

$$VO^{2+} + V^{2+} + 2H^+ \rightarrow 2V^{3+} + H_2O \quad (9) \qquad VO_2^+ + 2V^{2+} + 4H^+ \rightarrow 3V^{3+} + 2H_2O \quad (10)$$

Concentration of protons was calculated with following equation [14]:

$$c_{H+}^{hc}(t) = c_{H+,init}^{hc} + c_5^{hc}(t) \quad (11)$$

The activation overvoltages η_{act} are difficult to identify, and for the sake of simplicity they can be added to the η_{ohm} by introducing equivalent resistance [17]:

$$\eta_{act}(t) + \eta_{ohm}(t) = \bar{R}_{ce,c/d} I(t) \quad (12)$$

where $\bar{R}_{ce,c/d}$ is the equivalent resistances of the cell, which value (experimentally determined) is different for charge and discharge.

The concentration overvoltages η_{con} can be calculated with the use of Nernst equation and application of Fick's law for estimation of diffusion rate [21]:

$$\eta_{con}(t) = \frac{GT}{F} ln\left(1 - \frac{I(t)}{k_m A_e F c_{react}^{hc}(t)}\right) \quad (13) \qquad \eta_{con,tot} = \left|\eta_{con}^{pe}\right| + \left|\eta_{con}^{ne}\right| \quad (14)$$

where c_{react} is the reactant concentration, which is presented in Table 1; k_m is a mass transfer coefficient at the electrode-electrolyte surface, which reflects the ratio of diffusion and convection for reacting species on the surface and inside the porous electrode and can be approximated with following equation:

$$k_m = \alpha 10^{-4} u^{\beta} \quad (15)$$

where α and β are empirical constants which depend on the cell topology (α=*1.6* and β=*0.4* for VRB flow-through cell [19,21]), and u is electrolyte velocity in the cell's channel ($u=Q/A_{ch}$) [26].

Table 1. Reactant concentration on the electrodes during charge and discharge

$c_{react}(t)$, mol L^{-1}	Charge	Discharge
Positive electrode	$c_4^{cell}(t)$	$c_5^{cell}(t)$
Negative electrode	$c_3^{cell}(t)$	$c_2^{cell}(t)$

The energy performances of the single VRB flow-by cell are evaluated by the *SOC(t)*, the Coulombic efficiency (*CE*), the voltage efficiency (*VE*) and the Energy Efficiency (*EE*) [22]:

$$SOC(t) = c_2(t) / \left(c_2(t) + c_3(t)\right) = c_5(t) / \left(c_5(t) + c_4(t)\right) \quad (17)$$

$$CE = \tau_d / \tau_c \quad (18) \qquad VE = \langle U_{ce,d} \rangle / \langle U_{ce,c} \rangle \quad (19) \qquad EE = CE \cdot VE \quad (20)$$

where τ_c and τ_d are the duration of the charge and discharge processes respectively.

The values of the input parameters used in the proposed mathematical model are reported in Table 2.

4. Experimental set up

The experimental set up, which main characteristics are summarised in Table 2, was based on an Arbin fuel cell hardware with double serpentine channel flow field design [13] and 5 cm^2 active area [22]. Nafion 115 was used as a membrane material.

Equal amounts (20 mL) of aqueous solutions containing 1.0M $VOSO_4$ + 2.5 M H_2SO_4 and 1.0 M $V_2(SO_4)_3$ + 2.5 M H_2SO_4 were used as negative and positive electrolyte, respectively. The electrolytes were stored inside two separate sealed reservoirs under high-purity argon atmosphere and were pumped through the cell by means of two peristaltic pumps. All the electrochemical measurements have been performed using an Autolab PGSTAT 302 potentiostat. The experiments were carried out in order to measure the charge-discharge and polarization curves.

Table 2. Specification of experimental set up and parameters in the simulation

Characteristics	Unit	Value
Faraday's constant, F	C mol^{-1}	96485
Standard reduction potential, U_0	V	1.259
Initial overall vanadium ions concentration in each half-cell, $c^{hc}_{van,init}$	mol L^{-1}	1.0
Tank volume, V_{tk}	L	$2.0 \cdot 10^{-2}$
Operating temperature, T	K	298.0
Initial proton concentration in each half-cell, $c^{hc}_{H+,init}$	mol L^{-1}	5.0
Electrode surface area, A_e	m^2	$5.0 \cdot 10^{-4}$
Graphite plate channels cross-section overall area, A_{ch}	m^2	$2.0 \cdot 10^{-6}$
Single half-cell volume, V_{hc}	m^3	$2.6 \cdot 10^{-7}$
Membrane thickness, d_m	m	$125 \cdot 10^{-6}$
Diffusion coefficients [23]		
D_2	$m^2\ s^{-1}$	$9.4 \cdot 10^{-12}$
D_3	$m^2\ s^{-1}$	$1.4 \cdot 10^{-11}$
D_4	$m^2\ s^{-1}$	$4.4 \cdot 10^{-12}$
D_5	$m^2\ s^{-1}$	$2.4 \cdot 10^{-12}$
Membrane porosity, ε [24]	-	0.2
Q_1, Q_2, Q_3	L s^{-1}	$0.7 \cdot 10^{-4}$, $2.5 \cdot 10^{-4}$, $8.6 \cdot 10^{-4}$

During charge-discharge curve measurements the cell was charged up to 1.6 V and discharged up to 0.8 V at fixed current densities of 20, 40, 60, 80 and 100 mA cm^{-2}. At the same time the electrolyte flowrate was fixed and was equal to Q_3. At least 3 charge-discharge cycles at each current density were performed.

Measurements of polarization curves were carried out from initial SOC = 0.53 for discharge mode. In fact, the *SOC* decreased with the growth of the current for each value of the flowrate [25]. The decrease of *SOC* was due to the limited amount of electrolyte in the tanks and it could be reduced by increasing the volume of electrolyte in the tanks. The polarization curves were obtained by changing the load current with the step 0.01 and were measured for three different flowrates: Q_1; Q_2 and Q_3.

5. Results and discussion

The model described in Sec. 3 was tuned in accordance with experimental data. On the first step, the experimental polarization curves were used in order to determine the internal losses parameters which mainly affect the cell voltage. On the second step, these parameters were used for simulation of cell voltage and estimation of cell performance during charge-discharge cycles.

Linear behavior of the polarization curves (Fig. 2) at low currents indicates that activation overvortalges during discharge is low. One of the possible reasons for that is high electrochemical surface area of the electrodes covered with carbon black (detailed description of the electrode preparation procedure is described in ref. [22]). Estimation of the equivalent resistance $\bar{R}_{ce,d}$ from the slope of the linear part of the curves yields 0.07 **Ω**, that is close to the pure ohmic resistance of the cell determined by the impedance measurements. Thus, activation losses during discharge are negligible and can be accounted for using simple current independent resistance.

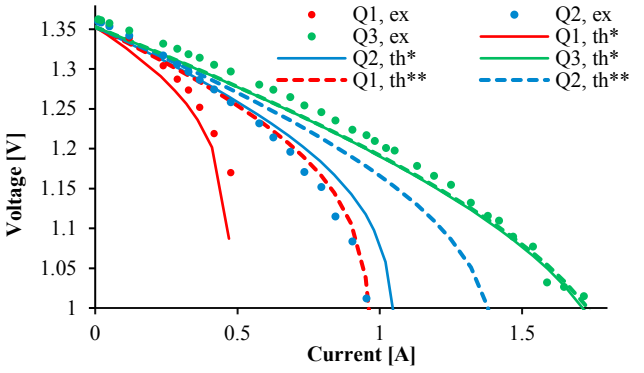

Fig. 2. Discharge polarization curves for different electrolyte flowrates corresponding to initial *SOC=0.53*. (* α=2, β=0.7; **α=1.6, β=0.4).

Influence of mass transfer limitations on the polarization curves was estimated with equations (13), (14) and (15). The calculations showed that the mass transfer coefficient with constants α and β generally available in the literature (α=1.6 and β=0.4) [19,21] is working well for high flowrate, but tends to overestimate the limiting current for lower flowrates. New values for α and β (α=2 and β=0.7) were found by fitting experimental polarization curves and used in further calculations.

Experimental charge-discharge curves show that charge and discharge cycles for different current densities start from different initial SOC. The initial value of SOC reaches 0 for charge and 1 for discharge at low current densities only. Higher currents cause higher overvoltages resulting in spurious side reactions such as hydrogen evolution or carbon corrosion, which decrease the capacity of the battery and limit the maximum and minimum SOC for charge and discharge. Different values for initial SOC have a great impact on the battery performance and need to be taken into account while modelling of VRB operation. To estimate initial SOC in the experiments we used Eq.(17), where the concentrations of vanadium species corresponded to the initial cell voltage were obtained from the solution of Nernst equation (4).

The investigations have shown that during discharge the crossover can be estimated by Fick's law for diffusion according to Eq. (5). However, the crossover can be neglected during charge (Fig 3.), that is in agreement with [24]. The vanadium ions transport across the membrane is governed not only by diffusion but also by the electric-filed-driven migration. The diffusion coefficients for V^{2+} and V^{3+} are larger than that for VO^{2+} and VO_2^+ ions. Therefore, the total diffusion flux is determined by diffusion fluxes of V^{2+} and V^{3+} and has a direction towards the positive half-cell during both charge and discharge. However, the migration fluxes have the same directions as the ionic current that have the trend towards to the negative half-cell during charge. Thus, having an opposite direction during charge process the diffusion and migration fluxes partially compensate each other and significantly decrease the crossover, which allows one to neglect crossover of vanadium ions through the membrane during charge of the battery.

The calculations have also revealed that equivalent cell resistance for charge curve is higher than 0.07 Ω and slightly depends on the applied current. The estimation of $R_{ce,c}$= 0.2 Ω (which is higher than $R_{ce,d}$ [25]) was carried out by the mathematical model (Sec. 3) in such a way that the theoretical charge curves fitted the corresponding empirical charge curves for all current densities with minor error. In particular, for $R_{ce,c}$= 0.2 Ω, the fitting was satisfactory at intermediate current densities, on the contrary the cell voltage was slightly underestimated and overestimated at low and high current densities, respectively.

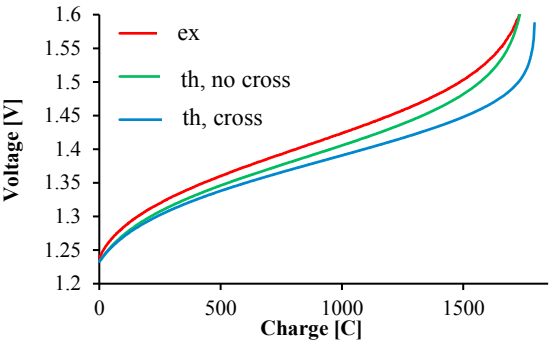

Fig. 3. Experimental and theoretical charge curves in presence and absence of crossover flux (for I/A_e = 40 mA/cm^2 and $Q_3 = 8.6 \cdot 10^{-4}$ L s^{-1}).

Despite of the assumed simplifications, the calculations fit well with experimental data and can simulate charge-discharge curves. Fig. 4 shows charge-discharge curve for current density 80 mA cm^{-2} and flowrate Q_3 = 0.86 mL s^{-1} (average calculation error is less than 2%).

The proposed model can estimate the performance of the cell rather well for current densities up to 80 mA cm^{-2}, however it tends to overestimate the columbic and energy efficiency of the cell at higher currents (Fig. 5). This is

likely caused by the fact that spurious side reactions (like hydrogen evolution or carbon corrosion) are more pronounced at higher current densities resulting in decrease of experimentally observed coulombic efficiency. Since such side reactions are not considered in the model the calculations show longer discharge time than it is observed in the experiments.

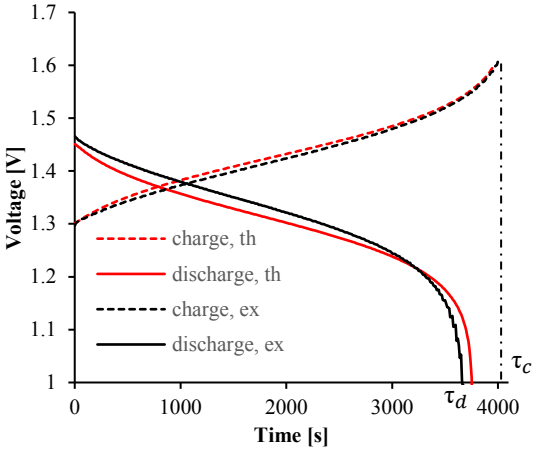

Fig. 4. Experimental and theoretical charge-discharge curves (for I/A_e = 80 mA/cm^2 and $Q_3 = 8.6 \cdot 10^{-4}$ L s^{-1}).

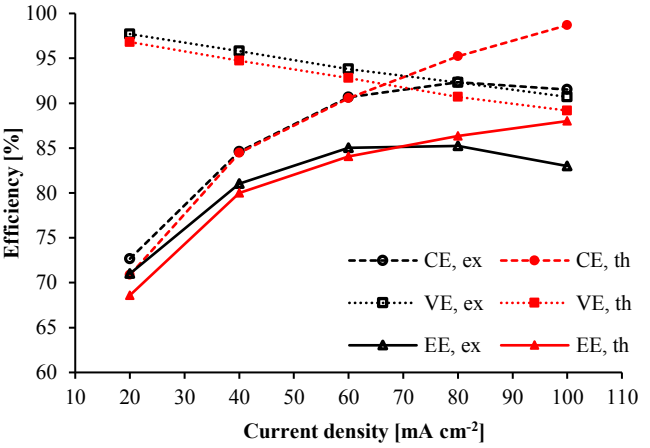

Fig. 5. Experimental and theoretical efficiencies of the single VRB flow-by cell for $Q_3 = 8.6 \cdot 10^{-4}$ L s^{-1} and with varying current density.

6. Conclusions

Main factors influencing the performance of Vanadium Redox Battery (VRB) flow cell were considered and systematically analyzed. The proposed simple model was compared with experimental data and demonstrated satisfactory results (with average error less than 3 %) in 20-80 mA cm^{-2} current density range. For higher currents, it slightly overestimates battery efficiency (by 7 %), that is mainly connected with the influence of spurious side reactions that were not considered in the model.

The study revealed that mass transfer limitations for cells with flow-by design are more affected by convection of reactive species than it was shown earlier in literature for flow-through cells. Based on experimental data, a new correlation for mass transfer constant was proposed.

Battery self-discharge is mainly determined by the crossover of vanadium ions through the membrane. Crossover of ions have a significant effect on the cell voltage during discharge and can be estimated by Fick's law of diffusion. At the same time, the crossover can be neglected during charge, due to the influence of electric-field-driven migration which compensate diffusion fluxes in charge process.

References

[1] U.S. Energy Information Administration. International Energy Outlook 2016. vol. 0484(2016). 2016. doi:www.eia.gov/forecasts/ieo/pdf/0484(2016).pdf.

[2] Baker JN, Collinson A. Electrical energy storage at the turn of the Millennium. Power Eng J 1999;13.

[3] Yang Z, Liu J, Baskaran S, Imhoff CH, Holladay JD. Enabling renewable energy-and the future grid-with advanced electricity storage. Jom 2010;62:14–23. doi:10.1007/s11837-010-0129-0.

[4] Rychcik M, Skyllas-Kazacos M. Characteristics of a new all-vanadium redox flow battery. J Power Sources 1988;22. doi:10.1016/0378-7753(88)80005-3.

[5] Aneke M, Wang M. Energy storage technologies and real life applications. A state of the art review. Appl Energy 2016;179:350–77. doi:10.1016/j.apenergy.2016.06.097.

[6] Yang Z, Zhang J, Kintner-Meyer MCW, Lu X, Choi D, Lemmon JP, et al. Electrochemical energy storage

for green grid. Chem Rev 2011;111:3577–613. doi:10.1021/cr100290v.
[7] Scamman DP, Reade GW, Roberts EPL. Numerical modelling of a bromide-polysulphide redox flow battery. Part 1: Modelling approach and validation for a pilot-scale system. J Power Sources 2009;189:1220–30. doi:10.1016/j.jpowsour.2009.01.071.
[8] Huskinson B, Marshak MP, Suh C, Er S, Gerhardt MR, Galvin CJ, et al. A metal-free organic–inorganic aqueous flow battery. Nature 2014;505:195–8. doi:10.1038/nature12909.
[9] Luo X, Wang J, Dooner M, Clarke J. Overview of current development in electrical energy storage technologies and the application potential in power system operation. Appl Energy 2015;137:511–36. doi:10.1016/j.apenergy.2014.09.081.
[10] Menictas C, Skyllas-Kazacos M. Performance of vanadium-oxygen redox fuel cell. J Appl Electrochem 2011;41:1223–32. doi:10.1007/s10800-011-0342-8.
[11] Shigematsu T, Kumamoto T, Deguchi H, Hara T. Applications of a vanadium redox-flow battery to maintain power quality. IEEE/PES Transm Distrib Conf Exhib 2002;2:1065–70. doi:10.1109/TDC.2002.1177625.
[12] Perles T. Vanadium Market Fundamentals and Implications. Met. Bull. 28th Int. Ferroalloys Conf., 2012.
[13] Aaron DS, Liu Q, Tang Z, Grim GM, Papandrew AB, Turhan A, et al. Dramatic performance gains in vanadium redox flow batteries through modified cell architecture. J Power Sources 2012;206:450–3. doi:10.1016/j.jpowsour.2011.12.026.
[14] You D, Zhang H, Chen J. A simple model for the vanadium redox battery. Electrochim Acta 2009;54:6827–36. doi:10.1016/j.electacta.2009.06.086.
[15] Tang A, Bao J, Skyllas-Kazacos M. Thermal modelling of battery configuration and self-discharge reactions in vanadium redox flow battery. J Power Sources 2012;216:489–501. doi:10.1016/j.jpowsour.2012.06.052.
[16] Ashraf Gandomi Y, Aaron DS, Mench MM. Coupled Membrane Transport Parameters for Ionic Species in All-Vanadium Redox Flow Batteries. Electrochim Acta 2016;218:174–90. doi:10.1016/j.electacta.2016.09.087.
[17] Blanc C, Rufer A. Multiphysics and energetic modeling of a vanadium redox flow battery. 2008 IEEE Int Conf Sustain Energy Technol ICSET 2008 2008:696–701. doi:10.1109/ICSET.2008.4747096.
[18] Blanc C, Rufer A. Understanding the Vanadium Redox Flow Batteries 1989.
[19] Konig S, Suriyah MR, Leibfried T. Innovative model-based flow rate optimization for vanadium redox flow batteries. J Power Sources 2016;333:134–44. doi:10.1016/j.jpowsour.2016.09.147.
[20] Oh K, Won S, Ju H. A comparative study of species migration and diffusion mechanisms in all-vanadium redox flow batteries. Electrochim Acta 2015;181:238–47. doi:10.1016/j.electacta.2015.03.012.
[21] Tang A, Bao J, Skyllas-Kazacos M. Studies on pressure losses and flow rate optimization in vanadium redox flow battery. J Power Sources 2014;248:154–62. doi:10.1016/j.jpowsour.2013.09.071.
[22] Kondratenko MS, Karpushkin EA, Gvozdik NA, Gallyamov MO, Stevenson KJ, Sergeyev VG. In fl uence of aminosilane precursor concentration on physicochemical properties of composite Na fi on membranes for vanadium redox fl ow battery applications 2017;340:32–9. doi:10.1016/j.jpowsour.2016.11.045.
[23] Luo Q, Li L, Nie Z, Wang W, Wei X, Li B, et al. In-situ investigation of vanadium ion transport in redox flow battery. J Power Sources 2012;218:15–20. doi:10.1016/j.jpowsour.2012.06.066.
[24] Yang X-G, Ye Q, Cheng P, Zhao TS. Effects of the electric field on ion crossover in vanadium redox flow batteries. Appl Energy 2015;145:306–19. doi:10.1016/j.apenergy.2015.02.038.
[25] Aaron D, Tang Z, Papandrew AB, Zawodzinski TA. Polarization curve analysis of all-vanadium redox flow batteries. J Appl Electrochem 2011;41:1175–82. doi:10.1007/s10800-011-0335-7.